Impact of Vertical Atmospheric Structure on an Atypical Fire in a Mountain Valley

Mitsuhiro Ozaki [1],*, Rebecca M. B. Harris [2], Peter T. Love [2], Jagannath Aryal [3], Paul Fox-Hughes [4] and Grant J. Williamson [1]

[1] School of Natural Sciences, University of Tasmania, Hobart, TAS 7005, Australia; grant.williamson@utas.edu.au
[2] School of Geography, Planning, and Spatial Sciences, University of Tasmania, Sandy Bay, TAS 7005, Australia; r.m.b.harris@utas.edu.au (R.M.B.H.); p.t.love@utas.edu.au (P.T.L.)
[3] Department of Infrastructure Engineering, Faculty of Engineering and IT, The University of Melbourne, Melbourne, VIC 3010, Australia; jagannath.aryal@unimelb.edu.au
[4] Research and Development Branch, Bureau of Meteorology, Hobart, TAS 7000, Australia; paul.fox-hughes@bom.gov.au
* Correspondence: mitsuhiro.ozaki@utas.edu.au

Abstract: Wildfires are not only a natural part of many ecosystems, but they can also have disastrous consequences for humans, including in Australia. Rugged terrain adds to the difficulty of predicting fire behavior and fire spread, as fires often propagate contrary to expectations. Even though fire models generally incorporate weather, fuels, and topography, which are important factors affecting fire behavior, they usually only consider the surface wind; however, the more elevated winds should also be accounted for, in addition to surface winds, when predicting fire spread in rugged terrain because valley winds are often dynamically altered by the interaction of a layered atmosphere and the topography. Here, fire spread in rugged terrain was examined in a case study of the Riveaux Road Fire, which was ignited by multiple lightning strikes in January 2019 in southern Tasmania, Australia and burnt approximately 637.19 km^2. Firstly, the number of conducive wind structures, which are defined as the combination of wind and temperature layers likely to result in enhanced surface wind, were counted by examining the vertical wind structure of the atmosphere, and the potential for above-surface winds to affect fire propagation was identified. Then, the multiple fire propagations were simulated using a new fire simulator (Prototype 2) motivated by the draft specification of the forthcoming new fire danger rating system, the Australian Fire Danger Rating System (AFDRS). Simulations were performed with one experiment group utilizing wind fields that included upper-air interactions, and two control groups that utilized downscaled wind from a model that only incorporated surface winds, to identify the impact of upper air interactions. Consequently, a detailed analysis showed that more conducive structures were commonly observed in the rugged terrain than in the other topography. In addition, the simulation of the experiment group performed better in predicting fire spread than those of the control groups in rugged terrain. In contrast, the control groups based on the downscaled surface wind model performed well in less rugged terrain. These results suggest that not only surface winds but also the higher altitude winds above the surface are required to be considered, especially in rugged terrain.

Keywords: wildfire; rugged terrain; upper air interaction; AFDRS

1. Introduction

Recent fire events in Australia have highlighted the urgent necessity to develop better predictive models of fire behavior. Fires are important natural processes in many ecosystems. For instance, fires promote growth by introducing nutrients into the soil derived from the ashes produced, they can act as a successional disturbance, by removing competition and opening the canopies in forests, which encourages the establishment

of seedlings, and they can trigger seed germination. On the other hand, fires cause the destruction of human lives and property. For example, the Black Saturday Fires in 2009 killed 173 people and destroyed more than 2000 houses in Victoria, Australia, the Ash Wednesday Fires in 1983 resulted in 75 fatalities and the loss of 1900 houses in South Australia and Victoria, and the Black Tuesday Fires in 1967 cost 62 lives and destroyed 1300 houses in Tasmania [1–3]. In recent fires, the death toll from wildfires rose to 33 in the Black Summer fires between 2019 and 2020 in eastern Australia [4,5].

These fires propagated in not only flat or mild terrain but also mountainous areas [6–8]; yet, fires behave differently on slopes compared to flat or less topographically diverse regions. For instance, fires generally propagate more rapidly uphill than downhill [9] and it is often difficult to predict the fire spread and behavior in rugged terrain because the weather interacts with the more complex topography. For instance, such topography is favorable for thermally induced winds which often lead to unexpected fire behaviors [10]. In general, the solar radiation is higher, temperature is lower, humidity is lower, and the wind is stronger in mountainous areas than in lowlands [11,12]. These weather conditions also influence the fire propagation. Such interactions in rugged terrain often expose fire crews to greater risk when fighting fires in these areas than in flat or less rugged areas [13]. Additionally, these interactions pose a risk to tourists and people engaging in sports activities such as hiking and rock climbing in the mountains [14], as a fire spread direction may run contrary to expectations and the conditions may change rapidly. Further, the by-products of fires, such as smoke pollution, can have negative impacts on broad areas, including nearby densely populated regions [15]. For instance, smoke from wildfires and prescribed fires contains harmful particles for the respiratory organs and these pollutants are often referred to as atmospheric particulate matter (PM) and can be transported for long distances [4]; therefore, wildfires in mountainous areas can affect not only nearby locations but also distant areas.

Fire behavior is the result of interactions between the topography, fuel, and weather, such as the temperature, relative humidity, wind magnitude and direction [16,17]. In particular, wind plays a significant role in fire propagation in rugged terrain and exhibits various dynamic forms that strongly interact with the topography [11,16,18–21]. There are several dynamic wind forms of relevance to fire spread, including diurnal wind, pressure driven channeling, the downward transport of momentum and forced channeling. Diurnal winds occur when the micro-scale (<2 km) or meso-scale (2–200 km) atmospheric winds dominate while other dynamic winds are observed when the larger scale atmosphere is more influential [11]. On the other hand, the micro-scale atmosphere can also influence the larger scale atmosphere. For instance, nocturnal airflows subsiding from higher mountains frequently spread out and trigger mesoscale convective systems [22]. By contrast, forced channeling and pressure driven channeling result from synoptic scale atmospheric phenomena. Specifically, forced channeling is the result of a deflection of the geostrophic wind aloft by the surface topography. The direction of the forced channeling can suddenly shift by 180 degrees in response to even small changes in the geostrophic wind aloft. Meanwhile, pressure driven channeling results from the presence of a pressure gap within a valley, with the valley wind blowing from high to low pressure areas, and therefore is often known as a gap wind. Downward transfer of momentum is the dynamic wind caused by vertical mixing or gravity waves and is often observed with forced channeling. These upper winds may cause a fanning effect on the fire propagation in the valley, altering the rates and direction of spread in addition to the effect of the surface wind [10,19,23–25].

We present a case-study into fire behaviors in rugged terrain in Australia that will inform the development of a new generation of fire spread simulators. We aim to understand the impact of vertical atmospheric interactions on fire spread in rugged terrain. Two methodologies were employed: an examination of atmospheric cross-section plots, and a simulation of fire spread using the Prototype 2 simulator. A cross-section is a diagram that projects the elevated air in a vertical profile based on interpolated weather data. We used cross-section diagrams constructed for segments of the fire to quantitatively assess

the upper-air interactions. On the other hand, the Prototype 2 is a new fire simulator for fire propagation that has been implemented by following the draft specification of the Australian Fire Danger Rating System (AFDRS) [26].

The datasets required for these methodologies were fire isochrones, vegetation mapping, topographical and geological data, and the Bureau of Meteorology high-resolution Regional Reanalysis for Australia for Tasmania region (BARRA-TA). For the Prototype 2 simulations, three analysis groups were prepared with different types of wind to identify an impact of upper air interaction. The first was an experiment group which reflected the upper air interaction better than the other groups because the wind data are directly retrieved from BARRA-TA, which incorporates full, three-dimensional vertical wind modelling. The second and third were the control groups which contained the wind downscaled by WindNinja, a numerical diagnostic tool which improves the horizontal resolution of wind fields, but which does not directly ingest upper air. The difference between the two control groups was the parameterization of source wind data: the domain average initialization (WN-DAI) and gridded initialization (WN-GI). A wind was downscaled from a single location per time episode with the WN-DAI while a grid-based wind, which was reprojected from BARRA-TA, was generated with the other option, the WN-GI.

Our research aimed to determine whether upper air winds had greater impacts on a fire simulation in rugged terrain than in other, less topographically complex areas of the fire. The hypotheses to address the research objective were (1) conducive winds would be more frequently observed in rugged terrain than milder topography in the study area, and (2) the quality of the fire simulation would be lower in rugged terrain than in mild topography due to an inadequate consideration of the disruption of upper air. Note that there should be ideally only one variable changing in the comparison between the three groups, which is the influence of the upper air interaction among three groups; however, the spatial resolution also varies in BARRA-TA (1.5 km), WN-DAI (637 m) and WN-GI (447 m) due to their different preprocesses. Although the resolutions of the downscaled wind were finer and topographically more sensitive than that of the BARRA-TA dataset, these wind fields are less affected by upper air interaction. Indeed, there is an interface available for the ground surface level only in WindNinja 3.7.3; therefore, the experiment group based on BARRA-TA was expected to produce better results on the fire simulation when an upper air interaction took place. In other words, the simulations with WN-DAI, which was one of control groups, were expected to produce the lowest scores when the upper air interaction was active, since assimilated weather is ingested from only a single location per time episode.

2. Study Area, Methods, and Materials

2.1. Case Study

The case study area was the area burnt by the Riveaux Road Fire, in southern Tasmania, Australia, a location which includes a high topographic complexity, with multiple valleys within the fire ground and elevations of the ridges up to 1 km above sea level. The Riveaux Road Fire occurred during the summer of 2018–19, during the second warmest and driest February on record in Tasmania, Australia. Lightning strikes are the major source of natural fire ignition all over the world [27] and approximately 70 ignitions were confirmed among more than 2000 lightning strikes on the 15 January 2019 in southern Tasmania [28]. The Riveaux Road Fire was one of several fires occurring in the state over the summer and was ignited by multiple lightning strikes around the 15 January 2019. The final size of the fire was approximately 637.19 km^2 [6,29,30]. Interestingly, the fire did not propagate radially from a single ignition point, but rather multiple fires occurred, merged, and propagated almost along the valley axes as seen in Figure 1.

The burnt area contained highly fire sensitive vegetation, with approximately 68% of the affected vegetation having a fire sensitivity (describing the recovery period of vegetation after burning) that was classified as either extreme (6.20%), very high (22.65%) or high (39.49%) impact, requiring, respectively, more than 500, 50, or 30 years to recover post-fire,

according to recently published vegetation spatial data, TasVeg4 [6,31]. However, not all vegetation was killed by the fire, even under the severe intensity [32].
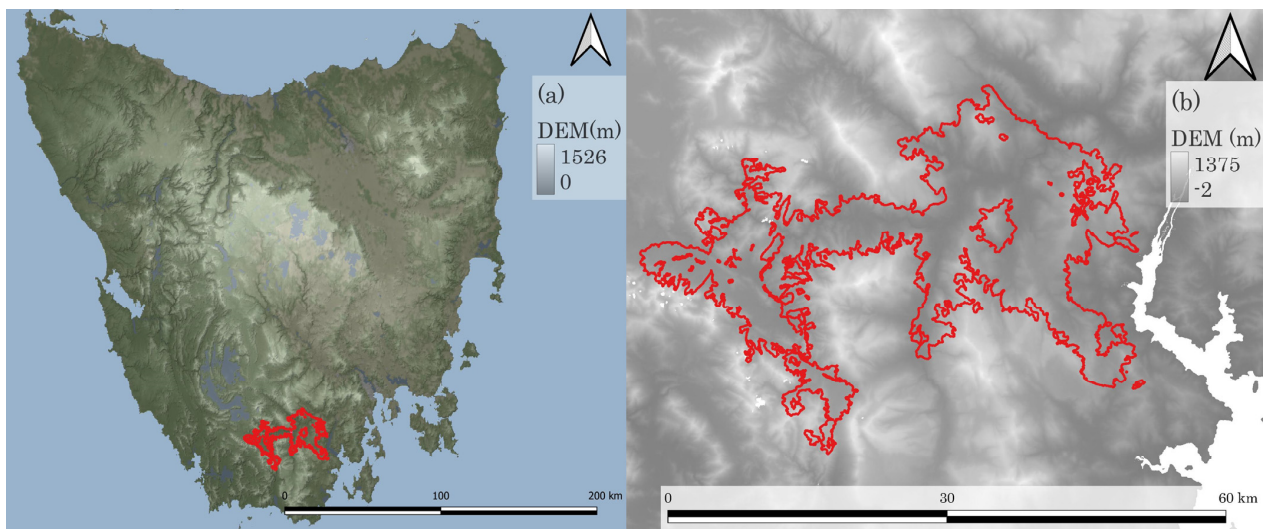
Figure 1. (**a**) Riveaux Road Fire is in southern Tasmania on the left subfigure; (**b**) this site is located in rugged terrain, in which the highest ridge near the fire is 1375 m and the fire ran along valley axes in gray, shown in the right subfigure.

2.2. Methods

This study employed a range of methods to investigate the behavior of the Riveaux Road Fire and the role of topography. Firstly, cross-section diagrams were employed to identify the conducive wind structures, which are defined as the combination of wind and temperature layers likely to result in enhanced surface wind, by profiling the atmosphere vertically to confirm the association of ruggedness with an upper air interaction. Secondly, fire spread simulations under a range of modelled wind fields were carried out with Prototype 2, the successor of the fire simulator, Prototype 1 [33]. The core fire models embedded in Prototype 2 are those in the Australian Fire Danger Rating System (AFDRS) with some modification. The quality of the fire simulations was verified using a fractions skill score (FSS) and confusion matrices. A key aspect of fire simulation in rugged terrain is how an upper air interaction is incorporated and cross-section diagrams and these simulation methods were expected to show the influence of upper air on the fire simulation in rugged terrain.

2.2.1. Atmospheric Profile

Cross sections are functions that ingest the atmospheric grid data and interpolate a weather grid between specific locations along a specified dimension. The output diagrams allow the identification of atmospheric states such as wind vectors, the geopotential height of an atmospheric pressure layer and atmospheric stability, by showing data along a sliced vertical plane [34]. The Bureau of Meteorology high-resolution Regional Reanalysis for Australia for the Tasmanian region (BARRA-TA) was ingested in this case study. Firstly, vertical atmospheric profiles were plotted during the fire periods for each available fire isochrone. There are three patterns to draw a cross-section. (1) The coordinates are altitudinal and either longitudinal or latitudinal. (2) The orientation can be along or perpendicular to ridges or valleys, depending on the topographical features. In addition, (3) there are two types of wind direction: tangential or normal to a target region; therefore, all eight combinations of the cross-section series were plotted in each isochrone during the fire periods. Secondly, the number of plots was visually counted, with 1525 plots in total for all isochrones. The length of the time series depends on the duration of fire. For instance, the duration of the actual fire in isochrone #1 was four days (Section 2.3.1); therefore, 24 h were multiplied by four days and eight patterns with one extra hour before and after the

duration, which became $784 = (1 + 24 \times 4 + 1) \times 8$. Thirdly, percentages of the plots containing conducive structures, which exhibit significantly dynamic wind changes of speed and/or direction above 900 hPa due to the combination of wind and temperature layers, were calculated by dividing by the total number of plots in each isochrone. These atmospheric pressure levels were selected because the elevation of each fire isochrone was situated at around 950 hPa, and, therefore, the impacted areas could be covered by these atmospheric pressure levels.

2.2.2. Prototype 2

Fire danger rating systems are helpful to communicate with the corresponding fire communities such as researchers and operators to share their awareness of fires [26]. Prototype 2 is a successor to the previous Prototype 1 model, which employed three polygon-based geometries with three granularities of prediction polygons, and was previously demonstrated to predict the fire spread in the 2016 Lake Mackenzie fire in Tasmania [33]. The Prototype 2 also follows the specification of the Australian Fire Danger Rating System (AFDRS) in terms of Australian fuel sub-models and was applied here to the Riveaux Road fire. The architecture of Prototype 2 is addressed in Section S2.1.1 in File S1. Prototype 2 extends on the previous Prototype 1 model by including the following features (Table 1).

Table 1. Prototype 2 features. Prototype 2 follows the specification of AFDRS about #1 which is further addressed in Table 2.

#	Prototype 2 Features
1	Inclusion of multiple fire spread models for specific vegetation types
2	Configuration of wind types
3	Various geometries of prediction polygons
4	Capability of multiple ignitions with different start times
5	Configuration of two types of downslope distances, which are calculations of distance with and without altitudinal gap
6	Adjustment of the rate of fire spread (ROS)
7	Configuration to stop a fire simulation
8	Simulation of spotting fire

Table 2. Eight fire models used in Prototype 2 with general fuel types [26].

#	General Fuel Type	Fire Model Name
1	Continuous grasslands	CSIRO Grassland fire spread model [35,36]
2	Grassy woodlands and open forests	CSIRO Grassland for northern Australia model [35,36]
3	Hummock grasslands	Desert spinifex model [37]
4	Buttongrass moorlands	Buttongrass moorlands model [38,39]
5	Shrubby dry eucalypt forests	Dry Eucalypt Forest Fire Model (DEFFM or Vesta) [40]
6	Semi-arid mallee heath	Mallee heath model [41]
7	Temperate shrublands	Heathland model [42]
8	Pine plantations	Adjusted Pine model [26]

An appropriate fire model was selected from the suite incorporated in the upcoming Australian Fire Danger Rating System (Table 2), depending on the vegetation type of the fire front location. Details of the fire models with vegetation types are addressed in Table S38 in File S1. Note that only some of the listed fire models, such as the CSIRO Grassland, Buttongrass moorlands model, Vesta, and Heathland models, are utilized in this study because only these vegetation counterparts were present in the study area.

Wind type, which is ingested to simulate fire propagation, is configurable in Prototype 2. There were a few types of wind in this study, for example, the BARRA-TA at a resolution of approximately 1.5 km, and downscaled wind fields generated by WindNinja at approximately 637 m (WN-DAI) and 447 m (WN-GI) [43,44]. The details of the wind preprocessing are described in Section 2.3.2.

There are several geometries available, such as Delaunay, diamond, hexagon, square and Voronoi, to map the prediction of fire and the reason for employing various geometries is to provide a range of samplings of fire propagation to increase the prediction accuracy. Note that a granularity of the prediction polygon was not always associated with accuracy in earlier work [33]. In addition, each prediction spatial polygon consists of various properties, such as the burn completion status and an elapsed time from the ignition time. This elapse property allows for tracking the fire propagation. The elapsed time is calculated from the fire rate of spread (ROS) using the distance between the centroids of the grid cell and the associated neighboring grid cell.

Fires can be ignited in multiple locations with various timings and be simulated to converge on each other. According to ignition data from the Tasmania Fire Service (TFS), the Riveaux Road Fire was ignited at 11 separate start points at differing times, and these ignition data were stored in the database as the basis of triggering the fire simulation starts. There is evidence that the coalescence of multiple fires can accelerate fire propagation in a non-linear fashion [45]; however, Prototype 2 does not yet consider this acceleration which incurs a high computational overhead.

It is possible to configure two types of downslope distances: a plan/projected (2D) and linear/ground (3D). The former is suitable for a large site and the latter for small or laboratory sized [9]. Both options were used for each experiment to identify the impact of these slope calculations on the sizes of the fire isochrones.

Prototype 2 includes a defined adjustment factor for the rate of fire spread (ROS) to account for variation in the distance to and the number of nearest neighboring simulation polygons, depending on the geometry type selected. Details of the calculation of the fire spread elapse and rate of spread adjustment are described in File S2, Section S5.10.

A condition to stop the fire simulation is configurable and it is possible to configure the model so that the simulation can stop by specifying the duration and/or the area. If the burnt area were equal to or greater than the observed data by configuration, then the simulation would stop; however, it would also stop if there were no condition, such as fuel, to keep spreading the fire regardless of the other configurations.

A spotting fire can not only ignite another fire but also accelerate the rate of a fire spreading on a slope [46]. The transported distance of firebrands from a Eucalypt forest can reach 20 to 30 km [1,47], and while Prototype 2 includes the functions for a probabilistic simulation of a spotting fire, the spotting function was disabled in this study area because there was neither an observation nor any report about spotting fires having had a significant impact at Riveaux Road, although the reasons for some ignitions remain unknown.

2.2.3. Verification

The fire simulations were verified by various metrics: a fractions skill score (FSS), confusion matrix, threat score, and Cohen's Kappa score. Here, the FSS and precision indicator in confusion matrix are introduced because the FSS provides an overall accuracy of fire simulations. The others are addressed in Section S6, File S2.

The fractions skill score (FSS) is a probabilistic statistical verification metric, where the score is computed not only from the value in a grid but also in a neighborhood, and it provides a threshold, above which the result is considered "useful". The usefulness was employed to count the valid results in the fire simulations. Note that a neighbor is defined as the grid next to another grid (File S2, Section S4.2.3). The equation below is proposed [48–50]:

$$\text{FSS} = 1 - \frac{\text{FBS}}{\text{N}^{-1} \cdot \sum_{i=1}^{N} \text{P}^2 + \text{N}^{-1} \cdot \sum_{i=1}^{N} \text{P}_0^2} \tag{1}$$

where N represents the number of neighbors and FBS stands for the Fractions Brier Score as defined below:

$$\text{FBS} = \text{N}^{-1} \cdot \sum_{i=1}^{N} (\text{P} - \text{P}_0)^2 \tag{2}$$

$$P = n^{-1} \cdot \sum_{i=1}^{n} p_i \qquad (3)$$

$$P_0 = n^{-1} \cdot \sum_{i=1}^{n} p_{0_i} \qquad (4)$$

where P is the average of the neighbors of prediction p and p itself and P_0 is the average of the neighbors of the observation p_0 and p_0 itself. The threshold of the usefulness is expressed in the below Equation (5) as:

$$FSS_{useful} = 0.5 + \frac{f_{obs}}{2} \qquad (5)$$

where f_{obs} is a coverage of the fire propagation in a ground truth over a domain, i.e., the ratio of the burnt area. Namely, FSS_{useful} indicates the minimum limit of the useful scale. The scale can be attributed to a skillful scale if the FSS is greater than FSS_{useful} [49].

Another metric is the confusion matrix. There are two raters: a prediction of fire and an observed fire. This metric, firstly, classifies agreement into four groups (Table 3).

Table 3. Binary confusion matrix contains four combinations adapted in [51].

		Predicted Fire	
		Predicted No	Predicted Yes
Observed Fire	Actual No	TN	FP
	Actual Yes	FN	TP

TN, FP, FN, and TP stand for true negative, false positive, false negative and true positive, respectively.

There are some indicators by combining the above four classes. Precision is one of the major indicators in a confusion matrix and denotes the degree of correct prediction. The following equation shows how much a simulated fire area situates in the actual fire area over the total simulated fire area:

$$Precision = \frac{TP}{TP + FP} \qquad (6)$$

2.3. Data Structure and Process

The coordinate system in this study area was GDA94 zone 55 unless mentioned explicitly. The modelling domain in that coordinate system was defined to extend beyond the mapped boundary of the Riveaux Road Fire (Figure 2).

The geographical data for both the simulation input and output were stored in the database so that Prototype 2 could view and update these data efficiently.

2.3.1. Fire Isochrones

Three fire isochrones, obtained from the Tasmanian Fire Service (TFS) [52], were analyzed as the observed fire data for the Riveaux Road Fire (Figure 2). All three isochrones were smaller than 10 km². Each isochrone contained one or two ignition points. Fire isochrone #2 and #3 contained a single ignition point while #1 contained two ignitions; however, the temporal interval between these ignitions was two days despite a close distance, of approximately 160 m, between them. They were contained either in the same prediction polygon or in adjacent prediction polygons because the resolution of the prediction polygons was close to 250 m; therefore, the impact of fire coalescence was marginal even if it occurred. Table 4 shows the duration, burnt area, and terrain ruggedness represented by an elevation gap between the lowest and the highest elevation for each fire isochrone, which is mapped in Figure 2. The terrain in fire isochrone #1 was the least rugged while #3 was the most rugged, based on the elevation gap.
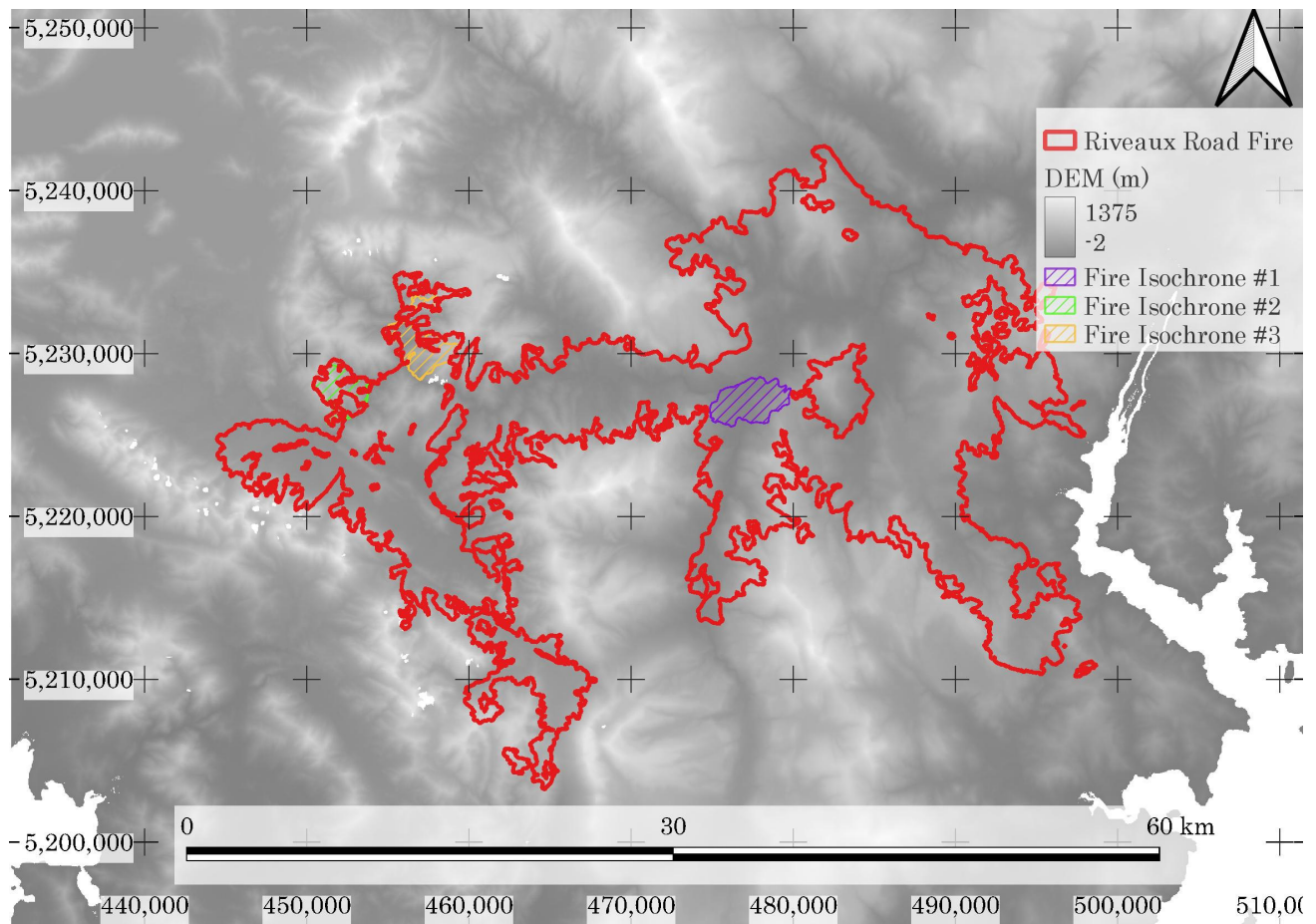
Figure 2. Extent of geospatial parameters for Riveaux Road Fire with three fire isochrones. Simulation was carried out over the entire domain represented in the image, beyond the observed fire boundary shown in red. Three fire isochrones were studied in this analysis: (#1) the east in purple occurred from the 18th in local time, (#2) the west isochrone in light green occurred from the 16th, and (#3) the north isochrone in orange started on the 20th.

Table 4. Fire isochrones with areas and elevations, listed from least to most rugged.

#	Start	End	Areas (km²)	Elevation Gap (Lowest: Highest) in Meters
1	18 January	22 January	9.94	335 (55:390)
2	16 January	24 January	6.17	571 (167:738)
3	20 January	24 January	9.77	619 (146:765)

2.3.2. Weather Datasets

The Bureau of Meteorology high-resolution Regional Reanalysis for Australia for the Tasmanian region (BARRA-TA) was the basis of the meteorology employed in this study. It includes various weather parameters, such as cloud coverage, precipitation, atmospheric pressure, temperature, geopotential height, soil moisture, relative humidity, and wind. Some of these weather data are two-dimensionally structured, while others are three-dimensional with the pressure level in addition to horizontal dimensions. The former contains surface wind, and the latter includes winds at 21 atmospheric pressure levels, except for the ground surface level. Three-dimensional wind data are useful to profile upper air by cross sections as addressed in Section 2.2.1 [53]. In addition to the raw BARRA-TA wind fields, wind was also downscaled using the numerical tool, WindNinja version 3.7.3, to increase the horizontal resolution and sensitivity of the winds to the topography [43]. WindNinja was used in two configurations to produce two wind fields utilized

by Prototype 2: the domain average initialization (WN-DAI) and gridded initialization (WN-GI). As a preprocess of wind for WN-DAI, weather of the central location of the study area was input into WindNinja per time step. In the case of WN-GI, the fully gridded surface wind in the BARRA-TA was reprojected from WGA84 to the local coordinates, GDA94. Although the WN-GI has not been officially announced at the present day, 1 May 2022, this option has been discussed and is available in public. These reprojected winds were ingested by WindNinja when the WN-GI was selected. The spatial resolutions of the BARRA-TA, WN-DAI and WN-GI were 1500 m, 637 m, and 447 m, respectively. Table 5 shows these wind types with their resolutions and features. All three resolutions are larger than those of the prediction polygons, which are roughly 250 m; therefore, the prediction polygons can cover the wind field to reflect the topographical sensitivity.

Table 5. Comparison of wind field models and resolutions used in fire simulation. Note that ρ indicates the percentage of the wind field containing upper air interaction directly.

Wind-Field	Resolution (m)	ρ (%)	Features
BARRA-TA	1500	100.00	Reanalysis by reflecting the real data
WN-DAI	637	<0.01	Downscaled from one wind seed from BARRA-TA per episode
WN-GI	447	8.88	Downscaled from gridded wind from BARRA-TA per episode

The original wind field data from the BARRA-TA was an approximately 1500 m spatial resolution. Although the resolution of the BARRA-TA is not sufficiently topographically sensitive to capture the horizontal dynamics of these wind-terrain interactions in comparison to the downscaled wind, the influence of the upper air interaction is higher than others (Table 5 and Figure 3); hence, the surface wind in this dataset was expected to reflect the vertical atmospheric interaction. On the other hand, the data downscaled by WindNinja were expected to reflect more topographical features with the diurnal activity at the ground surface level in addition to a finer resolution than the BARRA-TA dataset.

With regard to the configuration options influencing the downscaled wind field, there were common terrain-specific configurations selected in WindNinja. The first was the diurnal wind option, which allows the detection of the diurnal airflow in small valleys and requires geographical and temporal information in addition to meteorological data. This function takes into account the flow of surface heat, the vertical distance of the terrain, the slope and the amount of entrainment drag [44]. The second option was cloud cover, which can affect the magnitude of diurnal wind and atmospheric stability. Wind magnitude is reduced if cloud cover is high because the amount of insolation and temperature gap between day and night are lower under a cloud than with a clear sky [43,44]. The amount of cloud cover was retrieved from the BARRA-TA. The third configuration was non-neutral atmospheric stability, which represents the amount of atmospheric resistance against vertical motion and can substantially influence the flow of surface winds. In general, atmospheric stability is greatest at night [11]. The last was a conservation of mass (CoM), which can incorporate non-neutral stability, as a solver option [43].

2.4. Strategy to Find the Association of Terrain, Upper Air Interaction and Fire Simulation

There are a few steps to identify the association with topography, upper air interaction and fire propagation. Prior to the fire simulation, the atmospheric stability was measured by cross-section diagrams. Fire propagation was simulated in three groups with different wind types: BARRA-TA, the downscaled wind with domain average initialization (WN-DAI) and the downscaled wind with gridded initialization (WN-GI). The BARRA-TA was an experimental group because it contained upper air interaction without interpolation while the downscaled winds were classified as the control groups. Note that the resolution of the input gridded data of the WN-GI, 1.5 km, was nearly equivalent to the original data, namely, the BARRA-TA; however, the percentage of reanalysis wind to the downscaled wind was 8.88% because the output resolution was 447 m $\left(\frac{1500^{-2}}{447^{-2}} \approx 0.0888 \right)$, and the proportion of

reanalysis data in the WN-GI became much lower than in the BARRA-TA. Therefore, the WN-GI wind was ascribed as the control group.
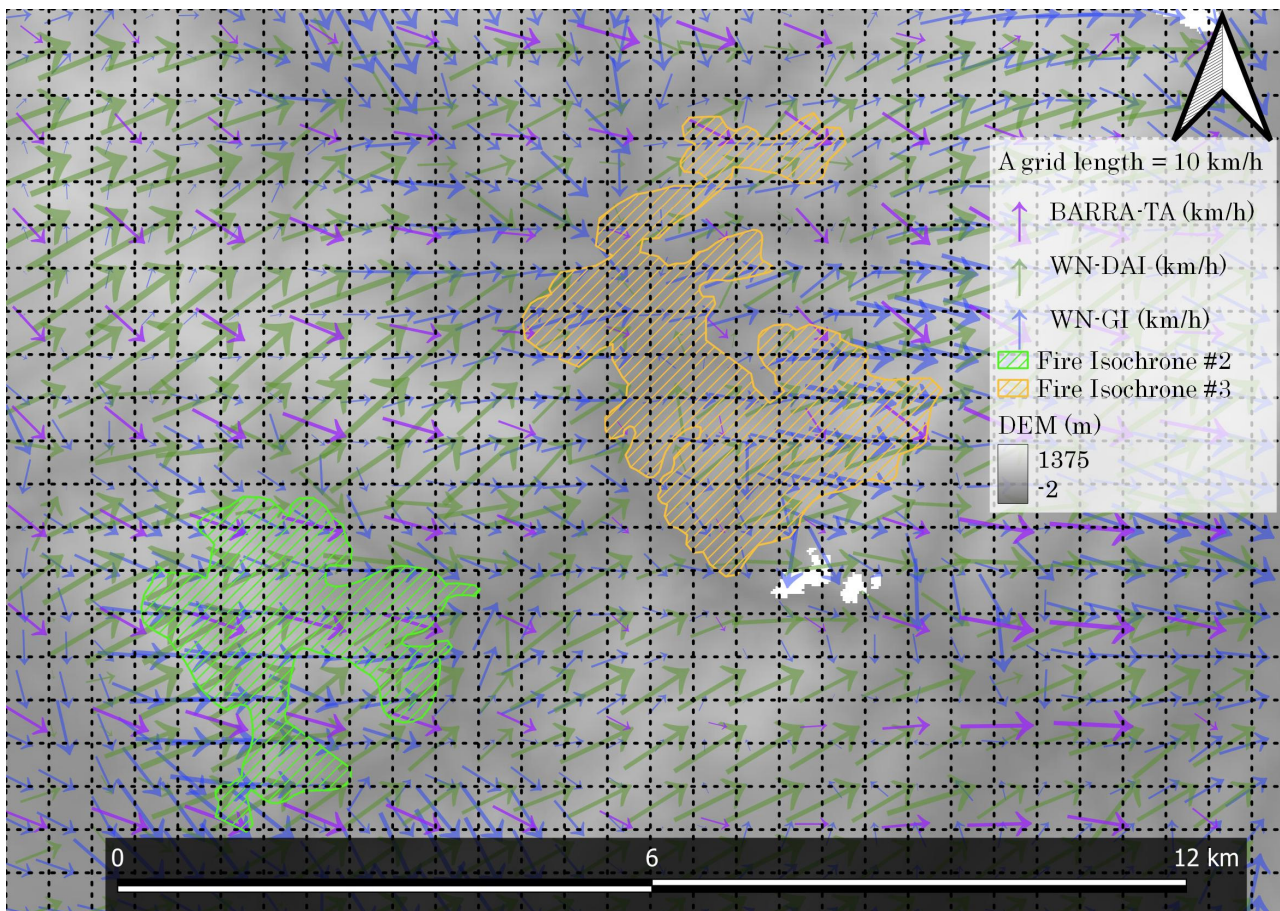
Figure 3. Three types of wind vectors at ignition, 22:00 on 20 January 2019 (Australia/Hobart), for fire isochrone #3: the surface wind in BARRA-TA in purple, the downscaled wind by WindNinja with domain average initialization (WN-DAI) in green and with grid initialization (WN-GI) in blue, are superimposed on a digital elevation model (DEM) with fire isochrone #2 and #3.

The fire was simulated for three fire isochrones (from #1 to #3), each of which was less than 10 km^2, and the quality of the simulations was assessed by three metrics. The first was the percentage of usefulness, whose fractions skill score (FSS) was greater than its threshold, "useful". The second was the median value of FSS. The last was precision, which was one of the main indicators in the confusion matrix.

3. Results

The terrain ruggedness appeared to be associated with the number of conducive structures. More conducive structures were observed in the rugged terrain than in the less rugged one. In addition, there was a different tendency of the simulation quality depending on the ruggedness of the terrain. The fire simulation with the BARRA-TA wind, which was assimilated wind, showed a better quality than with the downscaled wind in the rugged terrain despite the coarse spatial resolution. In turn, the simulations with the downscaled wind appeared better than with the BARRA-TA dataset in the less rugged terrain. The anomality of the fire simulation in the rugged terrain was endorsed by the number of prominent conducive structures. The details of the result are addressed in Section S3, File S1.

3.1. Atmospheric Profile

We found a tendency that the more rugged the terrain was, the more conducive structures were observed. The ruggedness showed a positive relationship with the number of conducive structures (Table 6). That is, the larger an elevation gap there was in a fire isochrone, the more conducive structures were observed.

Table 6. The percentage of conducive structure occurrence grouped by fire isochrone id (FI) with elevation gap (EG), and duration.

# FI	EG (m)	Duration (Days)	# Conducive Structures	# Time Steps	% Conducive Structures
1	335	4.0	51	784	6.51
2	571	8.5	185	1600	11.56
3	619	4.5	363	904	40.15

These conducive structures were least observed (6.51%) in isochrone #1 above 900 hPa, which was the least rugged terrain. Figure 4 shows monotonous and calm weather in isochrone #1. On the other hand, those winds were most observed (40.15%) in isochrone #3 which was the most rugged terrain. Figure 5 exhibits turbulent and unstable weather in isochrone #3.
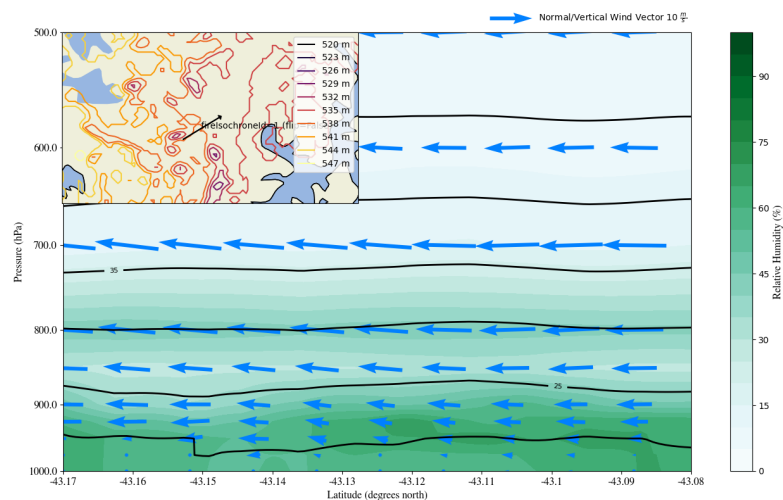
Figure 4. Example of cross section diagram for isochrone #1. Wind vectors are represented by blue arrows. The subfigure in the top-left pane shows the elevation contour for 950 hPa.
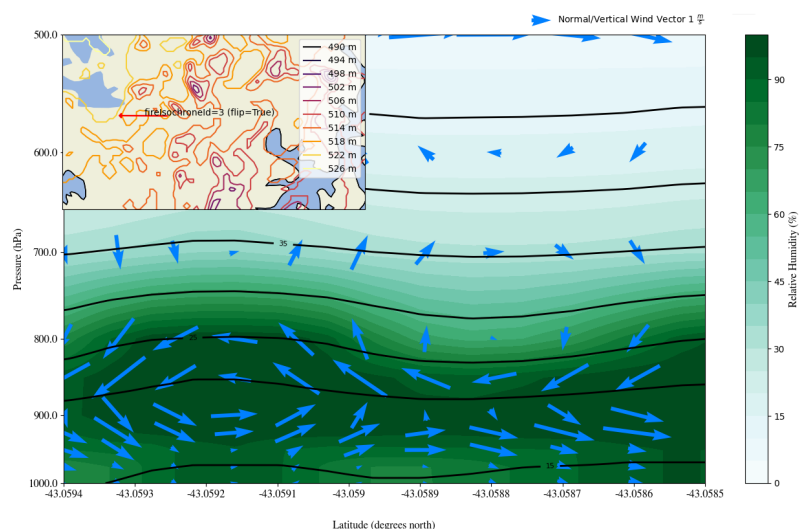
Figure 5. Example of cross section diagram for isochrone #3. Wind vectors are presented by blue arrow. The subfigure in the top-left pane shows the elevation contour for 950 hPa.

3.2. Fire Simulation

The fractions skill score (FSS) of the fire simulations varied with the ruggedness of terrain while there was not a significant difference in the precision. The simulation in fire isochrone #1, which was the least rugged terrain, had a higher FSS than the other isochrones when the downscaled winds were ingested. On the other hand, the simulations in #2 and #3, both of which were located in more rugged terrain, with the downscaled wind, showed a lower FSS than with the BARRA-TA wind. In contrast, the precision calculated from the confusion matrix did not show significant difference in the types of ruggedness. In the following subsections, the percentages of valid sample and median values of the FSS and precisions of the fire simulations are described. Note that the median values were calculated from ten samples, namely, five geometries for two types of downslope calculation.

3.2.1. Experiment Group (BARRA-TA)

Both the percentage of the useful fractions skills score (FSS) and median of FSS show the negative relationship with terrain ruggedness within a fire isochrone. Fire isochrone #1, which was in the least rugged terrain, showed a higher percentage of usefulness, 80%, and median FSS, 0.67, than the other isochrones. On the other hand, the precision scores were very similar to each other among the three isochrones ($\pm$0.3), each of whose precision indicated that approximately three-quarters of the simulated fire was in each fire isochrone when its simulation finished (Table 7).

Table 7. The number of valid samples grouped by fire isochrone id (FI) with elevation gap (EG), the percentage of the samples whose fractions skill score (FSS) exceeded the threshold, "useful", median value of FSS with "useful" in brackets and the precision in confusion matrix.

# FI	EG (m)	FSS Usefulness (%)	FSS Median (Useful)	Precision
1	335	80	0.67 (0.5)	0.72
2	571	70	0.52 (0.5)	0.73
3	619	50	0.50 (0.5)	0.75

Figure 6 shows an example of a fire simulation run with BARRA-TA wind using isochrone #1, the best predicted fire, 0.75, according to the fractions skill score (FSS). Although the fire was ignited on the west side of the isochrone, the fire well traced the historical data to the east.
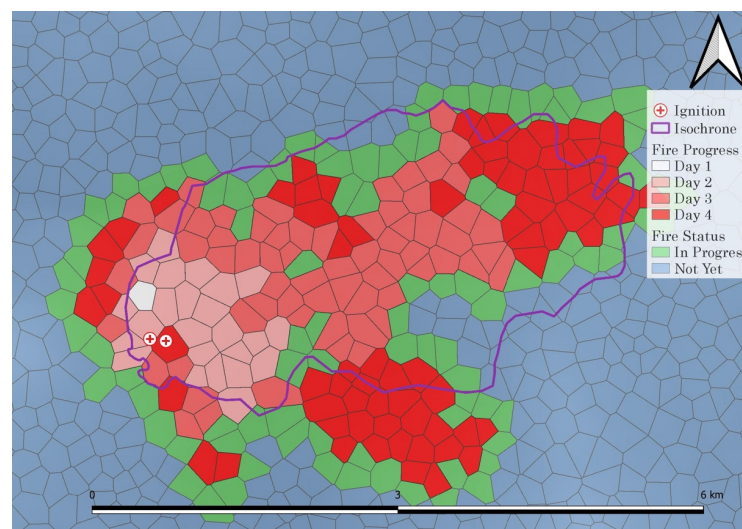
Figure 6. Example of a fire simulation run for isochrone #1. White to red colored Voronoi tessellation grids show burnt areas, green Voronoi indicate the fire front in progress at the end of the simulation, while observed isochrone is represented by the purple polygon. White cross icons indicate fire ignition points.

3.2.2. Control Group (WN-DAI)

In the same manner as the simulation with the BARRA-TA wind field, the fires were simulated with the downscaled data using domain average initialization (WN-DAI). Consequently, the percentage of usefulness in fractions skill score (FSS), and the median of both the FSS and precision show higher in fire isochrone #1 than in the other isochrones (Table 8).

Table 8. The number of valid samples grouped by fire isochrone id (FI) with elevation gap (EG), the percentage of the samples whose fractions skill score (FSS) exceeded the threshold, "useful", median value of FSS with "useful" in brackets and precision in confusion matrix. The FSS median in #2, which was 0.43, and #3, which was 0.49, did not reach the "useful" threshold, 0.5.

# FI	EG (m)	FSS Usefulness (%)	FSS Median (Useful)	Precision
1	335	90	0.68 (0.5)	0.75
2	571	40	0.43 (0.5)	0.68
3	619	40	0.49 (0.5)	0.74

On the other hand, the difference in precision between #1 and #3 was only 0.01. Figure 7 shows the fire simulation, in which the fractions skill score (FSS) was the lowest, 0.25.
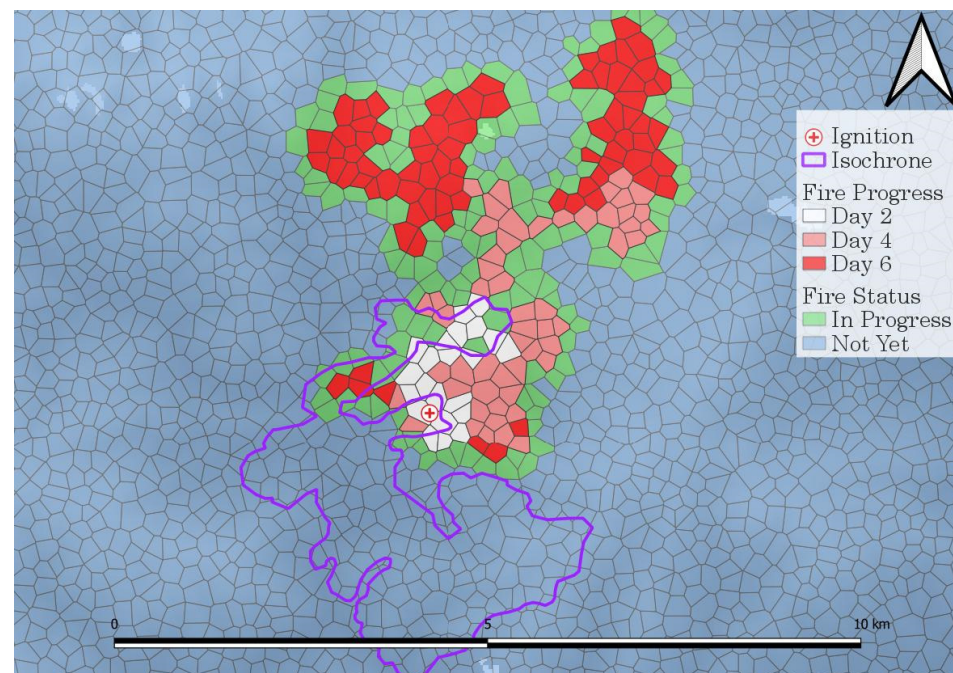
Figure 7. Example of fire simulation run for isochrone #2. White to red colored Voronoi grids show burnt areas, green Voronoi indicate the fire front in progress at the end of the simulation, while the observed isochrone is represented by the purple polygon. The fire ignited from a white cross icon in the middle of the figure.

3.2.3. Control Group (WN-GI)

In the same manner as the simulations with the other types of wind field, the fires were simulated with gridded initialization (WN-GI). Consequently, the percentage of usefulness in the fractions skill score (FSS) and median of the FSS in fire isochrone #1 showed significantly higher than in the other fire isochrones. On the other hand, there were only small differences in the precision metric (± 0.01) across the three simulations (Table 9).

Table 9. The number of valid samples grouped by fire isochrone id (FI) with elevation gap (EG), the percentage of the samples whose fractions skill score (FSS) exceeded the threshold, "useful", median value of FSS with "useful" in brackets and precision in confusion matrix. The median of FSS, which was 0.47, did not reach the "useful", 0.5, in fire isochrone #3, which was the most rugged terrain.

# FI	EG (m)	FSS Usefulness (%)	FSS Median (Useful)	Precision
1	335	100	0.63 (0.5)	0.71
2	571	50	0.51 (0.5)	0.70
3	619	20	0.47 (0.5)	0.70

3.3. Result Summary

The cross-section diagrams and Prototype 2 showed an association of the ruggedness of terrain, upper air interaction and the quality of the fire simulation. Table 10 concludes the fire simulation with an elevation gap as the ruggedness and the percentage of the conducive structures in the respective fire isochrones.

Table 10. Ground summary of the conducive structures and fire simulation with the types of wind. The number of valid samples are grouped by fire isochrone id (FI) with elevation gap (EG) indicating terrain ruggedness. Three right columns indicate the percentage of fractions skill score (FSS) which exceeded the threshold, "useful", for three types of winds: (1) BARRA-TA, (2) the downscaled wind by WindNinja with domain average initialization (WN-DAI), and (3) with gridded initialization (WN-GI). The values enclosed in brackets in these right columns indicate the medians of FSS.

# FI	EG (m)	Conducive Structure (%)	BARRA-TA	WN-GAI	WN-GI
1	335	6.51	80 (0.67)	90 (0.68)	100 (0.63)
2	571	11.56	70 (0.52)	40 (0.43)	50 (0.51)
3	619	40.15	50 (0.50)	40 (0.49)	20 (0.47)

4. Discussion

The fire models embedded in Prototype 2 ingest topography, fuel, and ground surface weather; however, it is also necessary to consider the vertical atmospheric interaction for fire simulation when synoptic or mesoscale weather is dominant or in rugged terrain. Three types of winds were ingested to simulate fire propagation. One was the coarse wind from BARRA-TA datasets, with a resolution of approximately 1.5 km. This dataset was reanalysis data, calculated using a sophisticated numerical weather prediction model and assimilated with historical weather parameters; therefore, various dynamic winds, such as diurnal wind, forced channeling and pressure driven winds, were represented within this wind field input. Although the other two wind fields downscaled by WindNinja were of a finer horizontal resolution than the BARRA-TA, and took into account the diurnal wind and atmospheric stability at the ground surface level, these fell short of the ability to model full, three-dimensional wind fields. Despite the higher resolution of the WindNinja output, the simulations with these downscaled wind fields showed a lower quality than the BARRA-TA in rugged terrain (Table 10).

First and foremost, the number of conducive structures was higher in more rugged terrain. The most conducive structures were observed as 40.15% in fire isochrone #3, in which there was the greatest elevation gap within the area, 619 m, among the three isochrones. This tendency agrees with the first hypothesis, that turbulent flows over the topography are more frequently observed in more rugged terrain.

Secondly, the quality of the fire simulation appeared mostly negatively related to the ruggedness and the number of conducive structures. For instance, the percentages of the fractions skill scores (FSS) were the best and the number of conducive structures was the least in isochrone #1, which was situated in the least rugged terrain, and this was consistent across all wind field models. This tendency partially confirms the second hypothesis. On the other hand, the FSS in #3 with the grid-based downscaled wind input (WN-GI), was

20%, which was poorer than the model parameterized with a single wind location input (WN-DIA), 40%, even though the former considered more assimilated data as a grid field than the latter; however, this gap is considered as marginal from the perspective of the median values of these FSS. In fact, these median values are very close each other, 0.49 and 0.47, with the WN-DAI and WN-GI, respectively, in fire isochrone #3, and both are less than the threshold, "useful"; therefore, the difference of the FSS between the WN-DAI and WN-GI is not reliable to confirm the second hypothesis thoroughly. The interpolation in the downscaled data is a result of fluid computation along the terrain, incorporating the diurnal wind and atmospheric stability at the ground surface level; however, upper weather can disrupt the surface flow, and this is not fully accounted for in the downscaled model. Diurnal wind is often subdued when synoptic or mesoscale wind is dominant. If the diurnal wind were dominant, the simulated fire would have agreed with the observed fire more. On the other hand, the dominance of larger scale weather is not always necessary in rugged terrain to intervene in the surface flow because upper air can interfere with it when there is a significant elevation gap from the adjacent location. For instance, if there is a weather station on a crest, which is surrounded by the upper air far above the neighbor's surface locations, the surface wind is affected by these surrounding winds aloft; however, the interpolated wind ingested by Prototype 2 did not reflect the upper air but was influenced by the surface factors nearby only.

Overall, it is necessary to consider the vertical atmospheric interaction in rugged terrain in the developing AFDRS. Although several efforts have been made in Prototype 2, an analysis of 10 m wind alone is not sufficient because the upper air appeared to affect the fire propagation. As a solution, it is necessary to acquire a finer-scale wind field than the BARRA-TA by incorporating upper air interactions. There are different advantages and drawbacks in each type of wind in the study case. Although the downscaled winds are of a finer resolution than the BARRA-TA, they do not fully incorporate upper air interactions. On the other hand, the BARRA-TA contains upper air interaction but is only available at a much coarser resolution. To improve the preprocessing of the wind field, it is necessary to investigate the upper air interaction in advance. In fact, there are various types of dynamic wind, such as forced channeling wind in mountainous regions; therefore, it is necessary to identify the types of dynamic wind in such an area. If the dynamic winds are incorporated at the preprocessing stage, it would be of some help to improve the fire prediction model in rugged terrain, and the improved model performance would be beneficial for fire crews in these areas to avoid collateral damages.

5. Limitations

The fire spread modelling undertaken in this study does have some limitations in the BARRA-TA, WindNinja, calculation of slope for the rate of fire spreading (ROS), fire coalescence, and the interaction of fire and atmosphere.

Firstly, the BARRA-TA has limitations for resolution and the accuracy of humidity modelling. In terms of the resolution of both the weather data and topography in the BARRA-TA, it was 1.5 km and coarser than the wind data downscaled by WindNinja and the digital elevation model (DEM), which was ingested to simulate fires and whose spatial resolution was approximately 27 m; however, it appears to be resolved enough to adequately profile the upper air. Indeed, the fire simulation parameterized with the BARRA-TA surface wind performed more accurately in rugged terrain than the finer downscaled winds; therefore, it partially achieved the purpose of this study despite a coarse spatial resolution. The BARRA-TA also includes 21 atmospheric pressure levels in the vertical atmospheric data, all of which contain parameters such as air temperature, relative humidity, and wind magnitude and direction [54]; however, there are known limitations in the ability of meteorological reanalysis models to capture the vertical distribution of humidity, due to the difficulty in deriving humidity from satellite models [55,56].

The second series of constraints are for WindNinja, a diagnostic tool to interpolate and downscale the wind data. For example, the Coriolis force is disregarded in WindNinja because the scale of the affected area is small [21,44].

The third limitation is the topographical coefficient on the rate of spread (ROS). In terms of the topographical effect on the ROS, Prototype 2 provides two calculations about the downslope distance: the plan/projected and linear/ground katabatic slope. The plan/projected slope distance is, in general, suitable for large areas while the linear/ground katabatic slope is suitable for small scale simulations [9]. Because the threshold or criterion for which the slope distance is to be used is not articulated, the results with both distances are addressed in this study. Despite employing both methods, they did not show much difference of quality in this study [9]. The details of the results with these different slope distance methods are addressed in Section S3, File S1. Note that there is only one way of calculating the anabatic slope distance employed.

The fourth limitation is the treatment of fire coalescence, which is not considered in this study due to the high computational requirement, and which prevented the incorporation of the acceleration of fire propagation coalescence [45]. Fire isochrone #1 contained two ignition points whose distance was approximately 160 m, but as the duration gap between these was approximately two days, coalescence effects appear unlikely.

The last limitation is the fire–atmospheric interaction. A fire interacts with the atmosphere by driving convection, the fire coalescence mentioned above, and a coupled fire-atmosphere (CFA) model is expected to predict the fire behavior; however, a CFA was not employed due to the high computational intensity [57].

6. Conclusions

This study tackles some of the difficulties in predicting fire propagation in rugged terrain. Prototype 2 is implemented by following the specification of the Australian Fire Danger Rating System (AFDRS) with some original features. The study case showed the association of upper air interaction, ruggedness, and the performance of fire simulation. In addition to fire simulations, the number of conducive structures above 900 hPa was measured using cross-section diagrams which identified more dynamic winds aloft in rugged terrain than in mild terrain. Fire spread simulations driven by BARRA-TA, which incorporated upper-air interaction, also performed better in rugged terrain than the downscaled wind fields in the control groups that did not directly involve a vertical atmospheric interaction. The fire model units in Prototype 2 currently ingest weather data at the ground surface level only. These units appeared functional in flat or mild terrain; however, this study showed the necessity to consider the upper air interaction in rugged terrain. In future studies, it is necessary to identify the types of dynamic wind which have an impact on fire in rugged terrain.

Supplementary Materials: The following supporting information can be downloaded at: https://www.mdpi.com/article/10.3390/fire5040104/s1, File S1 and File S2.

Author Contributions: Conceptualization, R.M.B.H., P.T.L., J.A., P.F.-H. and M.O.; methodology, P.T.L., P.F.-H. and M.O.; software, P.T.L. and M.O.; validation, M.O.; formal analysis, M.O.; investigation, P.T.L., P.F.-H. and M.O.; resources, P.T.L. and P.F.-H.; data curation, M.O.; writing—original draft preparation, R.M.B.H., P.T.L., J.A., P.F.-H., G.J.W. and M.O.; writing—review and editing, R.M.B.H., P.T.L., J.A., P.F.-H., G.J.W. and M.O.; visualization, M.O.; supervision, R.M.B.H., P.T.L., J.A., G.J.W. and P.F.-H.; project administration, R.M.B.H.; funding acquisition, none. All authors have read and agreed to the published version of the manuscript.

Funding: Grant Williamson is funded by the NSW Bushfire Risk Management Research Hub, Department of Primary Industry and Environment, New South Wales, Australia.

Informed Consent Statement: Not applicable.

Data Availability Statement: TasVeg 3 and 4 and Fire history are available at Land Information System Tasmania (LIST) https://www.thelist.tas.gov.au/app/content/home) https://www.thelist.tas.gov.au/app/content/home (accessed on 19 August 2020). Curing data are available at Australian Bureau of Meteorology http://opendap.bom.gov.au:8080/thredds/catalog/curing_modis_500m_8-day/aust_regions/tas/tiff/catalog.html (accessed on 14 June 2020). DEM and Geology data are available at https://www.ga.gov.au/ (accessed on 6 February 2021). Relative Soil Moisture is available at https://eo-data.csiro.au/projects/awap/ (accessed on 26 July 2020). BARRA-TA, Lightning strikes or Fire Isochrone are not available in public for free.

Acknowledgments: We also thank three anonymous reviewers whose comments have helped to significantly improve this manuscript. We would especially like to acknowledge the contributions to this manuscript of R.M.B.H., who sadly passed away during the writing of this paper. She leaves a significant legacy to the fields of climatology and fire ecology and will be sorely missed.

Conflicts of Interest: The authors declare no conflict of interest.

References

1. Cruz, M.G.; Sullivan, A.L.; Gould, J.S.; Sims, N.C.; Bannister, A.J.; Hollis, J.J.; Hurley, R.J. Anatomy of a Catastrophic Wildfire: The Black Saturday Kilmore East Fire in Victoria, Australia. *For. Ecol. Manag.* **2012**, *284*, 269–285. [CrossRef]

2. Weber, D.; Moskwa, E.; Robinson, G.; Bardsley, D.; Arnold, J.; Davenport, M. Are We Ready for Bushfire? Perceptions of Residents, Landowners and Fire Authorities on Lower Eyre Peninsula, South Australia. *Geoforum* **2019**, *107*, 99–112. [CrossRef]

3. Whittaker, J.; Blanchi, R.; Haynes, K.; Leonard, J.; Opie, K. Experiences of Sheltering during the Black Saturday Bushfires: Implications for Policy and Research. *Int. J. Disaster Risk Reduct.* **2017**, *23*, 119–127. [CrossRef]

4. Vardoulakis, S.; Jalaludin, B.B.; Morgan, G.G.; Hanigan, I.C.; Johnston, F.H. Bushfire Smoke: Urgent Need for a National Health Protection Strategy. *Med. J. Aust.* **2020**, *212*, 349. [CrossRef]

5. Filkov, A.I.; Ngo, T.; Matthews, S.; Telfer, S.; Penman, T.D. Impact of Australia's Catastrophic 2019/20 Bushfire Season on Communities and Environment. Retrospective Analysis and Current Trends. *J. Saf. Sci. Resil.* **2020**, *1*, 44–56. [CrossRef]

6. Land Information System Tasmania LISTMap. Available online: http://maps.thelist.tas.gov.au/listmap/app/list/map (accessed on 18 May 2020).

7. Wilson, A.A.G.; Ferguson, I.S. Fight or Flee?—A Case Study of the Mount Macedon Bushfire. *Aust. For.* **1984**, *47*, 230–236. [CrossRef]

8. Forsyth, D.; Gormley, A.; Woodford, L.; Fitzgerald, T. *Effects of the Black Saturday Fires on Sambar Deer Occupancy and Abundance: Black Saturday Victoria 2009–Natural Values Fire Recovery Program*; Department of Sustainability and Environment: Heidelberg, Australia, 2011.

9. Sullivan, A.L.; Sharples, J.J.; Matthews, S.; Plucinski, M.P. A Downslope Fire Spread Correction Factor Based on Landscape-Scale Fire Behaviour. *Environ. Model. Softw.* **2014**, *62*, 153–163. [CrossRef]

10. Kossmann, M.; Sturman, A.; Zawar-Reza, P. Atmospheric Influences on Bush Fire Propagation and Smoke Dispersion over Complex Terrain. In Proceedings of the Australasian Bushfire Conference, Christchurch, New Zealand, 3–6 July 2001; pp. 3–6.

11. Whiteman, C.D. *Mountain Meteorology: Fundamentals and Applications*; Oxford University Press: New York, USA, 2000; ISBN 0-19-803044-4.

12. Sharples, J.; Mills, G.; McRae, R. Extreme Drying Events in the Australian High-Country and Their Implications for Bushfire Risk Management. *Aust. Meteorol. Oceanogr. J.* **2012**, *62*, 157–170. [CrossRef]

13. Sharples, J.J.; McRae, R.H.D.; Weber, R.O. An Empirical Probabilistic Study of Wind Direction over Complex Terrain. In Proceedings of the 18th World IMACS/MODSIM Congress, Cairns, Australia, 13–17 July 2009; pp. 4446–4452.

14. Clivaz, C.; Langenbach, M. Organisation and Professional Development of Mountain Guides and Leaders in Tourist Regions: The Swiss Case Compared with the French Experience. *J. Outdoor Recreat. Tour.* **2020**, *29*, 100257. [CrossRef]

15. Iqbal, N.; Ahmad, S.; Kim, D.H. Towards Mountain Fire Safety Using Fire Spread Predictive Analytics and Mountain Fire Containment in Iot Environment. *Sustainability* **2021**, *13*, 2461.

16. Noble, I.R.; Gill, A.M.; Bary, G.A.V. McArthur's Fire-danger Meters Expressed as Equations. *Aust. J. Ecol.* **1980**, *5*, 201–203. [CrossRef]

17. Griffiths, D. Improved Formula for the Drought Factor in McArthur's Forest Fire Danger Meter. *Aust. For.* **1999**, *62*, 202–206. [CrossRef]

18. Zardi, D.; Whiteman, C.D. Diurnal Mountain Wind Systems. In *Mountain Weather Research and Forecasting*; Springer: New York, NY, USA, 2013; pp. 35–119.

19. Sharples, J.J. An Overview of Mountain Meteorological Effects Relevant to Fire Behaviour and Bushfire Risk. *Int. J. Wildland Fire* **2009**, *18*, 737–754. [CrossRef]

20. Bushfire Cooperative Research Centre (CRC) Phoenix—A Fire Charateristic Mapping Model. Available online: https://www.bushfirecrc.com/sites/default/files/managed/resource/posterproga-tolhurst.pdf (accessed on 5 December 2020).

21. Forthofer, J.M. Modeling Wind in Complex Terrain for Use in Fire Spread Prediction. Master's Thesis, Colorado State University, Fort Collins, CO, USA, 2007; 130p.

22. Houze Jr, R.A. Orographic Effects on Precipitating Clouds. *Rev. Geophys.* **2012**, *50*, 1. [CrossRef]
23. Whiteman, C.D.; Doran, J.C. The Relationship between Overlying Synoptic-Scale Flows and Winds within a Valley. *J. Appl. Meteorol.* **1993**, *32*, 1669–1682. [CrossRef]
24. Smedman, A.-S.; Bergström, H.; Högström, U. Measured and Modelled Local Wind Field over a Frozen Lake in a Mountainous Area. *Contrib. Atmos. Phys.* **1996**, *69*, 501–516.
25. Smedman, A.-S.; Bergström, H. An Experimental Study of Stably Stratified Flow in the Lee of High Mountains. *Mon. Weather Rev.* **1995**, *123*, 2319–2333. [CrossRef]
26. The Australasian Fire and Emergency Service Authorities Council (AFAC) Australian Fire Danger Rating System—Research Prototype. Available online: https://www.afac.com.au/initiative/afdrs/afdrs-publications-and-reports (accessed on 19 May 2020).
27. Couto, F.T.; Salgado, R.; Guiomar, N. Forest Fires in Madeira Island and the Fire Weather Created by Orographic Effects. *Atmosphere* **2021**, *12*, 827. [CrossRef]
28. Wardlaw, T. Measuring a Fire. The Story of the January 2019 Fire Told from Measurements at the Warra Supersite, Tasmania. *Fire* **2021**, *4*, 15. [CrossRef]
29. Bureau of Meteorology Tasmania in Summer 2018-19: Very Warm and Mostly Dry. Available online: http://www.bom.gov.au/climate/current/season/tas/archive/201902.summary.shtml (accessed on 25 May 2020).
30. Blackwood, G.; Williams, K.; Ooi, C.S.; Hardy, A. Bushfires and Tourism: A Framing Analysis of Media Reportage of the 2019 Tasmanian Bushfire Season for Tourism Narratives. In Proceedings of the CAUTHE 2020: 20: 20 Vision: New Perspectives on the Diversity of Hospitality, Tourism and Events, Auckland, New Zealand, 10–13 February 2020; pp. 326–328.
31. Pyrke, A.; Marsden-Smedley, J. Fire-Attributes Categories, Fire Sensitivity, and Flammability of Tasmanian Vegetation Communities. *Tasforests* **2005**, *16*, 35–46.
32. Bowman, D.M.; Murphy, B.P.; Neyland, D.L.; Williamson, G.J.; Prior, L.D. Abrupt Fire Regime Change May Cause Landscape-Wide Loss of Mature Obligate Seeder Forests. *Glob. Chang. Biol.* **2014**, *20*, 1008–1015. [CrossRef] [PubMed]
33. Ozaki, M.; Aryal, J.; Fox-Hughes, P. Dynamic Wildfire Navigation System. *ISPRS Int. J. Geo-Inf.* **2019**, *8*, 194. [CrossRef]
34. May, R.M.; Arms, S.C.; Marsh, P.; Bruning, E.; Leeman, J.R.; Goebbert, K.; Thielen, J.E.; Bruick, Z.S. *MetPy: A Python Package for Meteorological Data*; Unidata: Denver, CO, USA, 2020.
35. Cheney, N.P.; Gould, J.S.; Catchpole, W.R. Prediction of Fire Spread in Grasslands. *Int. J. Wildland Fire* **1998**, *8*, 1–13. [CrossRef]
36. Cruz, M.G.; Gould, J.S.; Kidnie, S.; Bessell, R.; Nichols, D.; Slijepcevic, A. Effects of Curing on Grassfires: II. Effect of Grass Senescence on the Rate of Fire Spread. *Int. J. Wildland Fire* **2015**, *24*, 838–848. [CrossRef]
37. Burrows, N.; Gill, M.; Sharples, J. Development and Validation of a Model for Predicting Fire Behaviour in Spinifex Grasslands of Arid Australia. *Int. J. Wildland Fire* **2018**, *27*, 271–279. [CrossRef]
38. Marsden-Smedley, J.B.; Catchpole, W.R. Fire Behaviour Modelling in Tasmanian Buttongrass Moorlands i. Fuel Characteristics. *Int. J. Wildland Fire* **1995**, *5*, 203–214. [CrossRef]
39. Marsden-Smedley, J.B.; Catchpole, W.R. Fire Behaviour Modelling in Tasmanian Buttongrass Moorlands II. Fire Behaviour. *Int. J. Wildland Fire* **1995**, *5*, 215–228. [CrossRef]
40. Cheney, N.P.; Gould, J.S.; McCaw, W.L.; Anderson, W.R. Predicting Fire Behaviour in Dry Eucalypt Forest in Southern Australia. *For. Ecol. Manag.* **2012**, *280*, 120–131. [CrossRef]
41. Cruz, M.G.; McCaw, W.L.; Anderson, W.R.; Gould, J.S. Fire Behaviour Modelling in Semi-Arid Mallee-Heath Shrublands of Southern Australia. *Environ. Model. Softw.* **2013**, *40*, 21–34. [CrossRef]
42. Anderson, W.R.; Cruz, M.G.; Fernandes, P.M.; McCaw, L.; Vega, J.A.; Bradstock, R.A.; Fogarty, L.; Gould, J.; McCarthy, G.; Marsden-Smedley, J.B. A Generic, Empirical-Based Model for Predicting Rate of Fire Spread in Shrublands. *Int. J. Wildland Fire* **2015**, *24*, 443–460. [CrossRef]
43. Firelab WindNinja Tutorials Version 3.6.0. Available online: https://weather.firelab.org/windninja/tutorials/ (accessed on 1 April 2022).
44. Forthofer, J.; Shannon, K.; Butler, B. Simulating Diurnally Driven Slope Winds with WindNinja. In Proceedings of the 8th Symposium on Fire and Forest Meteorological Society, Boston, MA, USA, 13–15 October 2009; 13p.
45. Hilton, J.; Sharples, J.; Sullivan, A.; Swedosh, W. Simulation of Spot Fire Coalescence with Dynamic Feedback. In Proceedings of the 22nd International Congress on Modelling and Simulation, Hobart, Tasmania, Australia, 3–8 December 2017.
46. Storey, M.A.; Price, O.F.; Almeida, M.; Ribeiro, C.; Bradstock, R.A.; Sharples, J.J. Experiments on the Influence of Spot Fire and Topography Interaction on Fire Rate of Spread. *PLoS ONE* **2021**, *16*, e0245132. [CrossRef] [PubMed]
47. Hall, J.; Ellis, P.F.; Cary, G.J.; Bishop, G.; Sullivan, A.L. Long-Distance Spotting Potential of Bark Strips of a Ribbon Gum (Eucalyptus Viminalis). *Int. J. Wildland Fire* **2015**, *24*, 1109–1117. [CrossRef]
48. Ebert, E.E. Fuzzy Verification of High-Resolution Gridded Forecasts: A Review and Proposed Framework. *Meteorol. Appl.* **2008**, *15*, 51–64. [CrossRef]
49. Ebert, E.E. Neighborhood Verification: A Strategy for Rewarding Close Forecasts. *Weather Forecast.* **2009**, *24*, 1498–1510. [CrossRef]
50. Faggian, N.; Roux, B.; Steinle, P.; Ebert, B. Fast Calculation of the Fractions Skill Score. *Mausam* **2015**, *66*, 457–466. [CrossRef]
51. Markham, K. Simple Guide to Confusion Matrix Terminology. Available online: http://www.dataschool.io/simple-guide-to-confusion-matrix-terminology/ (accessed on 8 April 2018).
52. Tasmanian Fire Service Tasmania Fire Service. Available online: http://www.fire.tas.gov.au/ (accessed on 17 May 2020).

53. Eizenberg, N.; Jakob, D.; Fox-Hughes, P.; Steinle, P.; White, C.; Franklin, C. BARRA v1.0: Kilometre-Scale Downscaling of an Australian Regional Atmospheric Reanalysis over Four Midlatitude Domains. *Geosci. Model Dev.* **2021**, *14*, 4357–4378. [CrossRef]

54. Jakob, D.; Su, C.-H.; Eizenberg, N.; Kociuba, G.; Steinle, P.; Fox-Hughes, P.; Bettio, L. An Atmospheric High-Resolution Regional Reanalysis for Australia. *Bull. Aust. Meteorol. Oceanogr. Soc.* **2017**, *30*, 16.

55. Vey, S.; Dietrich, R.; Rülke, A.; Fritsche, M.; Steigenberger, P.; Rothacher, M. Validation of Precipitable Water Vapor within the NCEP/DOE Reanalysis Using Global GPS Observations from One Decade. *J. Clim.* **2010**, *23*, 1675–1695. [CrossRef]

56. Bock, O.; Parracho, A.C. Consistency and Representativeness of Integrated Water Vapour from Ground-Based GPS Observations and ERA-Interim Reanalysis. *Atmos. Chem. Phys.* **2019**, *19*, 9453–9468. [CrossRef]

57. Peace, M.; Charney, J.; Bally, J. Lessons Learned from Coupled Fire-Atmosphere Research and Implications for Operational Fire Prediction and Meteorological Products Provided by the Bureau of Meteorology to Australian Fire Agencies. *Atmosphere* **2020**, *11*, 1380. [CrossRef]